S-Tapered Fiber Sensors for Highly Sensitive Measurement of Refractive Index and Axial Strain

Rui Yang, Yong-Sen Yu, Chao Chen, Yang Xue, Xu-Lin Zhang, Jing-Chun Guo, Chuang Wang, Feng Zhu, Bao-Lin Zhang, Qi-Dai Chen, and Hong-Bo Sun, *Member, IEEE*

***Abstract*—An S-tapered fiber sensor has been realized on the common single-mode fiber by a fusion splicer. The S fiber taper (SFT) can be considered as a compact fiber Mach-Zehnder interferometer with the total length of hundreds of microns. The spectral characteristics of the SFTs with different structure parameters including axial offsets and taper waist diameters have been studied. Sensing experiments have also been carried out to test their response to refractive index (RI) and axial strain. The SFT with an axial offset of 114 μm and a taper waist diameter of 54.6 μm exhibits the best combination property. Its RI sensitivity reaches as high as 2066 nm/RI unit in the RI range of 1.407–1.421 and the average strain sensitivity is -183.4 pm/$\mu\varepsilon$, which is the highest strain sensitivity, to the best of our knowledge, with one or two orders of magnitude larger than the existing fiber strain sensors.**

***Index Terms*—Fiber optic sensors, fiber taper, Mach-Zehnder interferometer (MZI), refractive index sensors, strain sensors.**

I. Introduction

RECENTLY, optical fiber sensors have been extensively studied in measurement of various physical and chemical parameters, such as temperature [1]–[5], curvature [6], strain [7]–[12], and refractive index (RI) [13]–[25], due to their merits of small size, light weight, fast response, and corrosion resistance. Many kinds of the fiber sensor structures have been developed, for example, fiber Bragg gratings (FBGs) [16]–[18], long period fiber gratings (LPFGs) [12]–[15], and variety of optical fiber interferometers [2], [10], [25]. The FBGs are suitable for distributed sensing and they have high detecting resolution, but in RI measurement, they usually need to be chemical etched, greatly reducing the FBGs strength and durability. The LPFG-based RI sensors are robust and they have a high sensitivity when the surrounding RI (SRI) is close to that of the fiber cladding, but they also have a large cross sensitivity to temperature and bending. Furthermore, these fiber-grating-based (FBGs and LPFGs) sensors generally require precise and expensive fabrication techniques, including phase mask and laser source. The other fiber sensors based on interferometers, such as Fabry-Perot interferometers (FPIs) [10], [11], Mach-Zehnder interferometers (MZIs) [1], and Michelson interferometers (MIs) [25], are formed through some novel methods and structures in recent years. The microcavity- or microbubble-based fiber FPIs [10], [11], which are fabricated by a fusion splicer, have been reported to measure the axial strain. These fiber sensors have a simple and easy fabrication process, but their strain sensitivities are not satisfyingly high. Otherwise, the fiber MZIs and MIs for RI sensing have been realized by nonadiabatically tapering the fiber through a fiber-taper machine (flame brushing method) or a fusion splicer (arc discharging method). The nonadiabatic fiber tapers are used for coupling light energy from the fundamental core mode to cladding modes or reverse. The taper-based fiber interferometer sensors have many advantages, such as simple structure, ease of fabrication, and cost effectiveness, but their RI sensitivities are relative low and the total length of the structure is generally tens of millimeters, which is not compact for integrated applications.

Lately, we reported on a novel fiber sensor for RI and axial strain sensing based on a single "S"-like fiber taper [26], which is fabricated by applying off-axis pull while tapering the fiber in a fusion splicer. The S fiber taper (SFT) can be considered as a compact fiber MZI structure with a length of less than 1 mm. Its RI sensitivity is much higher than the normal fiber-taper-based MZIs and the axial strain sensitivity is even one or two orders of magnitude higher than the existing fiber strain sensors.

In this paper, we demonstrate the detailed characteristics of the SFTs fabricated under different experimental conditions, including different axial offsets of the two fiber holders and different discharging time. The change of the experimental conditions leads to different geometrical parameters (axial offset and taper waist diameter), which are used for controlling the transmission spectra and detection sensitivities of the SFTs. The highest RI sensitivity is 2124 nm/RI unit (RIU) in the RI range of 1.407–1.421 when the axial offset and the taper waist diameter of the SFT are 138 μm and 65.0 μm, respectively. When the axial offset is 114 μm and the waist diameter is 54.6 μm, we obtain the highest axial strain sensitivity of -183.4 pm/$\mu\varepsilon$, which is 3 times larger than our previous result. The SFT is a promising fiber sensor structure for highly sensitive measurement of SRI and axial strain or the other physical, chemical, and biological parameters, which can be obtained through measurements of RI or strain.

II. Fabrication

The SFT was fabricated on a common telecom single-mode optical fiber (SMF-28e, Corning, Inc.) by using an Ericsson FSU-975 fusion splicer. First of all, a user-defined fiber tapering program was created and only the step PULL 1 was chosen in the tapering process. The discharge current was set as 10 mA and the tapering time changed from 11 s to 15 s in the experiments. The axial offset of the two fiber holders in fusion splicer

Manuscript received May 03, 2012; revised July 03, 2012; accepted July 26, 2012. Date of publication August 02, 2012; date of current version September 26, 2012. This work was supported in part by National Natural Science Foundation of China (Grant #91123027, 90923037).

The authors are with State Key Laboratory on Integrated Optoelectronics, College of Electronic Science and Engineering, Jilin University, Changchun 130012, China (e-mail: yuys@jlu.edu.cn; hbsun@jlu.edu.cn).

Digital Object Identifier 10.1109/JLT.2012.2210997

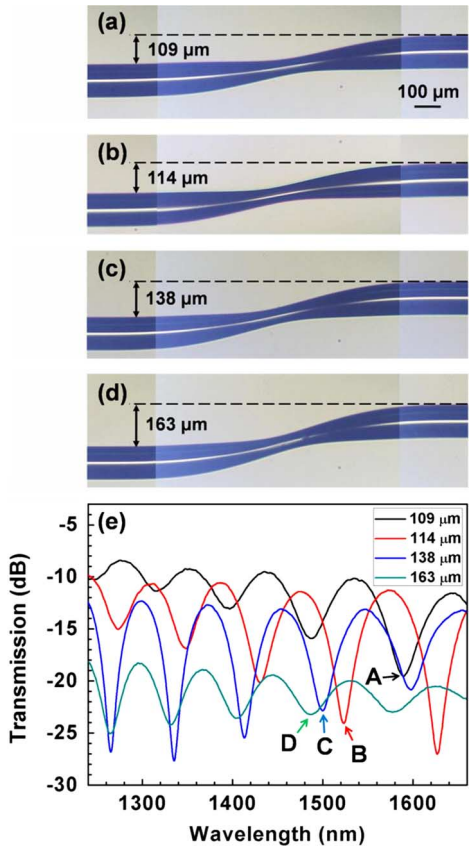

Fig. 1. (a)–(d) Optical microscope images of the SFTs with different axial offsets when the taper waist diameters are fixed to 65 μm. (e) Transmission spectra of the SFTs corresponding to (a)–(d).

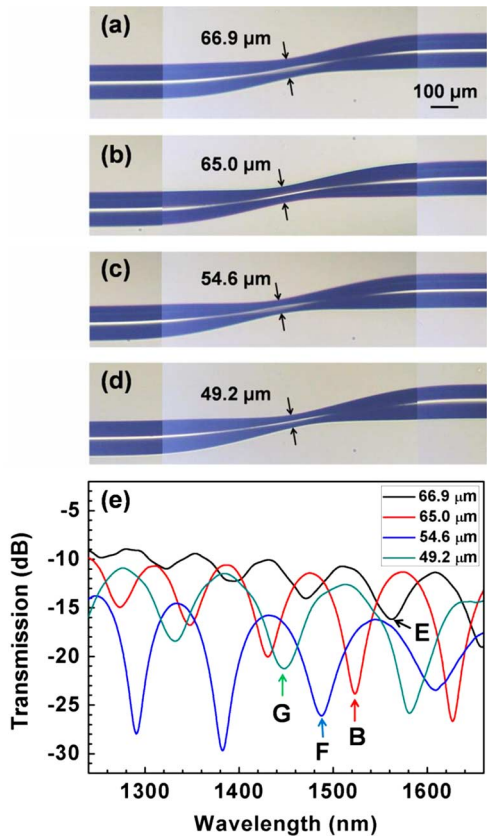

Fig. 2. (a)–(d) Optical microscope images of the SFTs with different taper waist diameters when the axial offsets are fixed to 114 μm. (e) Transmission spectra of the SFTs corresponding to (a)–(d).

could be adjusted manually with the help of a pair of cleaved fiber tips. After the axial offset was fixed, the fiber tips were replaced with a section of coating removed fiber sample. Two ends of the fiber sample were connected to an optical spectrum analyzer (OSA) (Yokogawa AQ6370B) and a supercontinuum broadband light source (Superk Compact, NKT Photonics, Inc.), respectively, to monitor the transmission spectrum.

The optical microscope images and transmission spectra of the SFTs fabricated under different experimental conditions are shown in Figs. 1 and 2 with different axial offsets and taper waist diameters, respectively. The SFTs in Figs. 1(a)–(d) have the axial offsets changing from 109 μm to 163 μm with the same tapering time of 12 s. The total lengths and taper waist diameters of the SFTs have the same values of about 700 μm and 65.0 μm, respectively. The corresponding transmission spectra are shown in Fig. 1(e). The insertion loss, which is mainly due to the fiber microbending loss, of the SFT increases with the axial offset augments and the extinction ratios (attenuation difference of maximum and minimum value) of the loss peaks are weaker when the axial offsets are too small (less than 109 μm) or large (greater than 163 μm). In our experiments, the taper length and taper waist diameter are correlation, namely a taper length corresponding to a taper waist diameter. Here, we chose the taper waist diameter to clarify the SFTs' transmission and sensing features. Figs. 2(a)–(d) show the SFTs with different taper waist diameters varied from 66.9 μm to 49.2 μm under the tapering time of 11 s, 12 s, 14 s, and 15 s, respectively. These SFTs have the same axial offset of 114 μm. Their corresponding transmission spectra are shown in Fig. 2(e). The number of attenuation peaks will decrease with the taper waist diameter thinned. In Figs. 1(e) and 2(e), the labeled peaks A–F with wavelengths around 1500 nm are used for comparison of the sensitivities of each SFT later. The fabrication process of the SFT has a good repeatability and this is crucial for the practical exploitation of the S-tapered architecture.

III. Theory

Fig. 3 shows the simulated light propagation in the SFT by Rsoft. The parameters of the S taper model are obtained from Fig. 1(b). The total length, axial offset and taper waist diameter are 700 μm, 114 μm, and 65.0 μm, respectively and the input wavelength is 1.55 μm. Light energy is largely coupled from the fiber core to cladding in the first bending section and partly coupled back from the cladding to core in the second one. A mount of light energy is coupled to cladding through the SFT and attenuated or absorbed by the fiber coating at last, leading to a relative large insertion loss of the structure. As mentioned above, the SFT can be considered as a novel fiber MZI structure. The two fiber bending sections play the role of coupling light from core mode to cladding modes or reverse. A higher-order

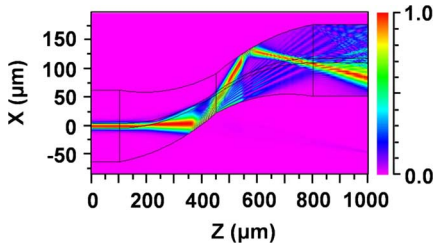

Fig. 3. Simulated light propagation in the SFT with total length of 700 μm, axial offset of 114 μm, and taper waist diameter of 65.0 μm, respectively, at the input wavelength of 1.55 μm.

cladding mode can be stimulated in the SFT due to the asymmetric structure [27]–[29]. We consider the simplest two modes interference process in the SFT and the form is

$$I = I_1 + I_2 + 2\sqrt{I_1 I_2}\cos(\Delta\Phi) \tag{1}$$

where I_1 and I_2 are the light intensities of the core and the cladding modes, and $\Delta\Phi$ is the phase difference between them. Here $\Delta\Phi$ is expressed as

$$\Delta\Phi = \frac{2\pi\Delta n_{\text{eff}} L_{\text{eff}}}{\lambda} \tag{2}$$

where Δn_{eff} is the effective RI difference between the core and the cladding modes, L_{eff} is the effective length of the interferometer, and λ is the input wavelength. When $\Delta\Phi$ becomes an odd times number of π, the attenuation peak wavelength λ_m can be expressed as

$$\lambda_m = \frac{2\Delta n_{\text{eff}} L_{\text{eff}}}{(2m+1)} \tag{3}$$

where m is the interference order. The formula $\Delta n_{\text{eff}} L_{\text{eff}}$ is the optical path length difference (ΔL_{opl}) of the concerned two modes. The free spectral range (FSR) $\Delta\lambda$ can be approximated by

$$\Delta\lambda \approx \frac{\lambda^2}{\Delta L_{\text{opl}}} \tag{4}$$

The transmission spectrum of the SFT has large FSR is owing to the small size, which results in a short ΔL_{opl}. The taper waist diameter has stronger impact on ΔL_{opl} than the taper length and a thinned taper waist makes a small ΔL_{opl}. That's why the loss peaks number decreases with the taper waist diameter diminish [Fig. 2(e)]. In addition, the extinction ratio of the SFT is mainly decided by the light energy distribution in the core and the cladding modes, namely I_1 and I_2. When the axial offset of the SFT is small, less energy will be coupled to the cladding mode and a small I_2 will weaken the interference in the end of the taper while for a large axial offset, little energy will be left in the core mode and the light interference is also weak, which are shown in Fig. 1(e).

IV. Sensing Experiments and Results

A. Temperature Sensing

In practical measurements of SRI and axial strain, the thermal characteristics of the SFTs are required and need to be compensated, so we investigated the temperature response of the SFT first of all. The SFT was mounted on a hot plate with a temperature resolution of 0.1°C. The hot plate was heated up from room temperature (20°C) to 100°C in steps of 10°C. The transmission spectra of the SFT are nearly unchanged at different temperatures, as shown in Fig. 4. The bottom wavelength of loss peak B just has a random fluctuation with temperature [Fig. 4(inset figure)]. We tested the other SFTs with different geometrical parameters and obtained the similar results. So the SFT is proper for the temperature independent SRI and strain sensing around room temperature.

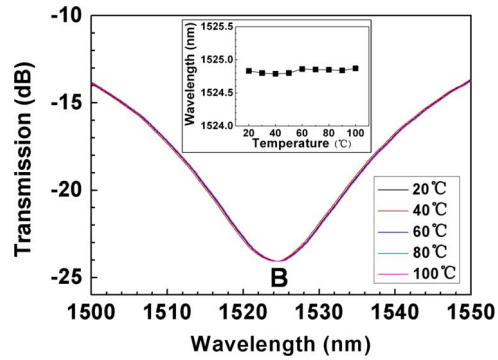

Fig. 4. Transmission spectrum of peak B changes with different temperature. Inset: wavelength of peak B changes with temperature.

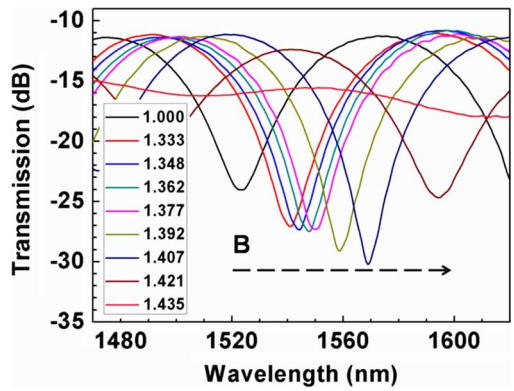

Fig. 5. Transmission spectrum of peak B changes with different SRI. The numbers denote to the SRI values.

B. SRI Sensing

RI measurements of the SFTs were carried out experimentally. Both ends of the SFT were fixed on a pair of fiber holders to keep it straight with no additional tension. In each measurement, only one drop of the RI solution was needed to test the SRI response due to the small size. After the transmission spectrum was recorded, the SFT was cleaned with ethanol and deionized water and dried by compressed air to recover its original spectrum in air. The procedure was repeated to measure the other RI solutions, which were made of different concentrations of glycerin water solution. The RI values of these solutions were collimated by an Abbe refractometer at 589 nm and room temperature °C. We choose peak B for example. Fig. 5 shows the typical transmission spectrum changes with different SRI. The spectrum of loss peak B moves to longer wavelength with SRI increasing due to the higher-order cladding mode taking part in

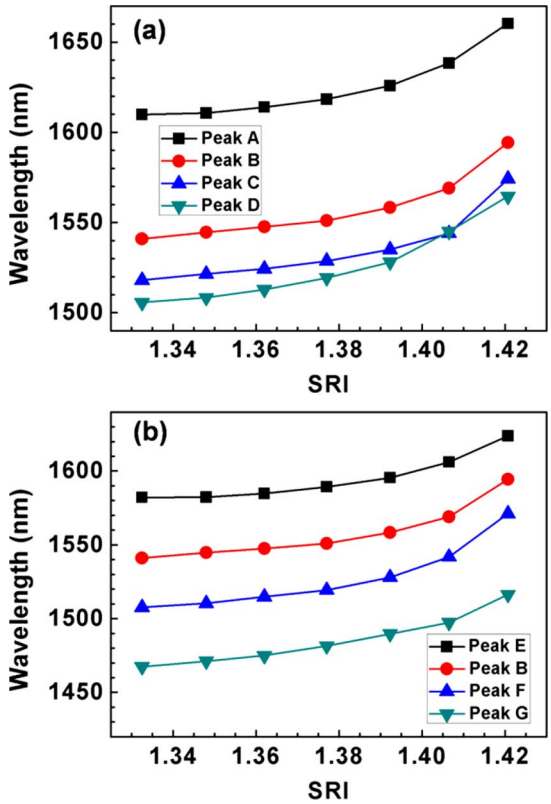

Fig. 6. Wavelength of attenuation peaks A–F shift as a function of SRI. Peaks in (a) and (b) belong to the SFTs with different axial offsets and taper waist diameters, respectively.

the light interference [14], [26]. When the SRI reaches the effective RI (ERI) of the cladding mode, light energy will spread out from this mode to environment and attenuate at last. With the cladding mode energy decreasing, light interference in the SFT is weakened, leading to the attenuation peaks becoming smaller and finally disappearing.

Fig. 6 shows the relationships between the wavelength of peaks A–F and different SRI. Peaks in Figs. 6(a) and (b) belong to the SFTs with different axial offsets and taper waist diameters, respectively. The loss peaks wavelength changes with SRI have a similar trend. The wavelength change rate becomes faster with the SRI increasing, which means the SFT has the highest RI sensitivity when the SRI closes to ERI of the cladding mode. The maximum SRI sensitivities of each SFT have been calculated and the results are shown in Fig. 9, denoted by the black solid squares. The highest RI sensitivity is 2124 nm/RIU in the RI range of 1.407–1.421, and the corresponding loss peak is the peak C.

C. Axial Strain Sensing

The SFT has an extremely high sensitivity for axial strain detection. The experiments of strain sensing were carried through applying axial tension to the SFTs by a piezoelectric tensometer with a tension error of 0.001 N. Fig. 7 shows the typical transmission spectrum changes with different axial tension. The loss peak B moves to shorter wavelength with the tension increasing. The axial tension not only elongates the SFT but also changes

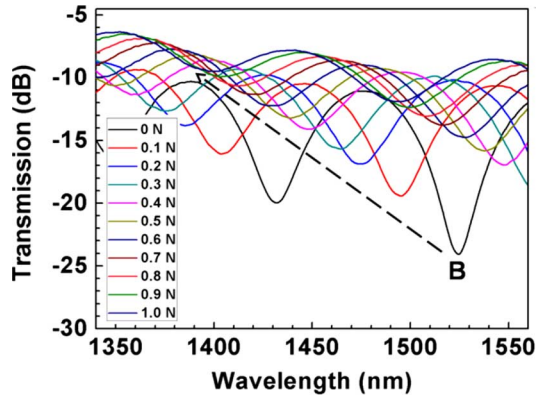

Fig. 7. Transmission spectrum of peak B changes with different axial tension.

the ERI of the fiber core and cladding modes. In our experiments, Δn_{eff} decreases much faster than the increment of the interferometer length L_{eff} when applied axial tension augments. According to the formula (3), the attenuation peak wavelength will have a blueshift with axial tension increasing. Furthermore, the shape of the SFT will change with axial tension. When the tension augments, the axial offset of the SFT will decrease, leading to more light energy remains in fiber core mode. So the light interference is weakened and the transmission power increases with the axial tension augments, which is shown in Fig. 7. We can calculate the axial strain inside the fiber by the formula

$$\varepsilon = \frac{F}{\pi r^2 E} \tag{5}$$

where F is the axial tension, r is the cladding radius, and E is the silica Young's modulus. The wavelength shifts of attenuation peaks A–F with axial strain are shown in Fig. 8. When the axial strain is small, the wavelength change is relative larger than the change at big strain. That maybe results from a large decrease of Δn_{eff}, which is induced by the fast shape change of the SFT when an axial strain applied in the fiber. The average strain sensitivities of the loss peaks A–F are also calculated and plotted in Fig. 9, represented by the blue solid circles. The highest strain sensitivity is -183.4 pm/$\mu\varepsilon$, which is 3 times larger than our previous result. The extremely high strain sensitivity is one or two orders of magnitude, to our best knowledge, higher than the existing fiber strain sensors.

In addition, we checked the polarization response of the SFT and found that the device is insensitive to polarization.

D. Discussion

Maximum SRI sensitivities (black solid squares) and average axial strain sensitivities (blue solid circles) of the peaks A–F are plotted in Fig. 9. The results in Fig. 9(a) approximately shows the sensitivities of the SFT with different axial offsets. When the axial offset is less than 138 μm, the maximum SRI sensitivity of the SFT increases with the axial offset augments. But the value will reduce if the axial offset is too large, e. g. greater than 163 μm. The similar situation happens in the taper waist diameter cases, which are shown in Fig. 9(b). The maximum SRI sensitivity of the SFT has the largest value of 2124 nm/RIU when the axial offset is 138 μm and the taper waist

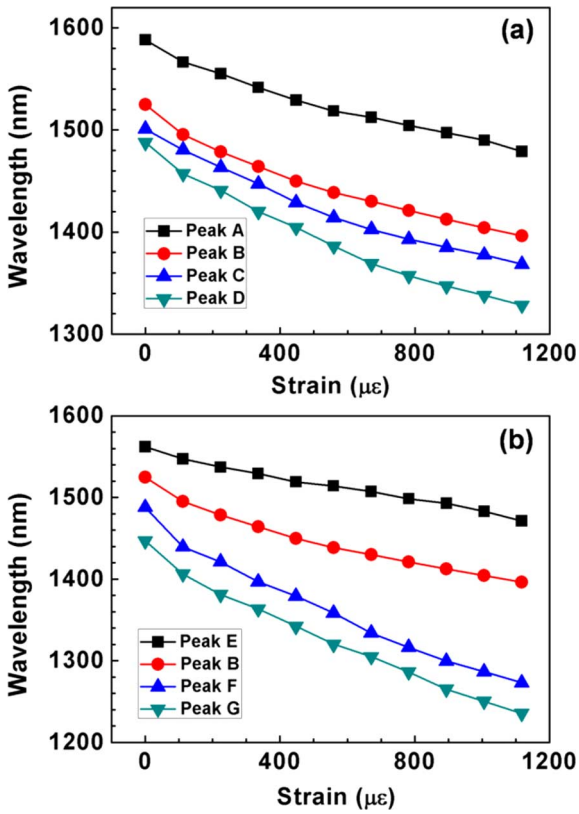

Fig. 8. Wavelength of attenuation peaks A–F shift as a function of axial strain. Peaks in (a) and (b) belong to the SFTs with different axial offsets and taper waist diameters, respectively.

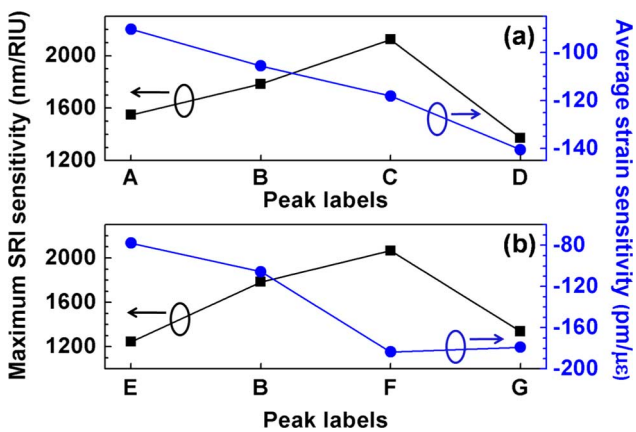

Fig. 9. Maximum SRI sensitivities and average axial strain sensitivities of the peaks A–F.

diameter is 65.0 μm. In the case of average strain sensitivity, the value decreases with the axial offset increasing [Fig. 9(a)]. When the taper waist diameter decreases, the strain sensitivity reduces firstly and then increases a little [Fig. 9(b)]. Considering the combination property, the best SFT with the highest SRI sensitivity of 2066 nm/RIU and average strain sensitivity of -183.4 pm/$\mu\varepsilon$, respectively, has the structure parameters of axial offset of 114 μm and the taper waist diameter of 54.6 μm. The sensing performances of the SFT are controllable through designing the taper structure parameters.

V. Conclusion

We have fabricated a series of SFTs under different experimental conditions and they are divided into two groups by axial offsets and taper waist diameters. The characteristics of the SFTs, especially their transmission spectra, have been analyzed in detail. Sensing experiments have been carried out to test their response to SRI and axial strain. The transmission spectrum of the SFT has a redshift with the SRI increasing and a blueshift with the axial strain increasing, respectively. The phenomenon of transmission spectrum weakened in the SRI and strain measurement has been observed and explained. The highest SRI sensitivity is 2124 nm/RIU in the RI range of 1.407–1.421 when the axial offset of the SFT is 138 μm and the taper waist diameter is 65.0 μm. The highest axial strain sensitivity of -183.4 pm/$\mu\varepsilon$, which is even 3 times higher than our previous result, is obtained with the axial offset of 114 μm and the taper waist diameter of 54.6 μm, respectively. In addition, the SFT also has many other advantages including small size, ease of fabrication, and low cost, which make it a promising fiber sensor in physical and chemical sensing fields.

References

[1] P. Lu and Q. Chen, "Asymmetrical fiber Mach-Zehnder interferometer for simultaneous measurement of axial strain and temperature," *IEEE Photon. J.*, vol. 2, no. 6, pp. 942–953, Dec. 2010.

[2] P. Lu, L. Men, K. Sooley, and Q. Chen, "Tapered fiber Mach-Zehnder interferometer for simultaneous measurement of refractive index and temperature," *Appl. Phys. Lett.*, vol. 94, no. 13, pp. 131110-1–131110-3, Apr. 2009.

[3] Y. Geng, X. Li, X. Tan, Y. Deng, and Y. Yu, "High-sensitivity Mach-Zehnder interferometric temperature fiber sensor based on a waist-enlarged fusion bitaper," *IEEE Sensors J.*, vol. 11, no. 11, pp. 2891–2894, Nov. 2011.

[4] D. Wu, T. Zhu, K. S. Chiang, and M. Deng, "All single-mode fiber Mach-Zehnder interferometer based on two peanut-shape structures," *J. Lightw. Technol.*, vol. 30, no. 5, pp. 805–810, Mar. 2012.

[5] C. Chen, Y. S. Yu, R. Yang, L. Wang, J. C. Guo, Q. D. Chen, and H. B. Sun, "Monitoring thermal effect in femtosecond laser interaction with glass by fiber bragg grating," *J. Lightw. Technol.*, vol. 29, no. 14, pp. 2126–2130, July 2011.

[6] D. M. Hernandez, A. M. Rios, I. T. Gomez, and G. S. Delgado, "Compact optical fiber curvature sensor based on concatenating two tapers," *Opt. Lett.*, vol. 36, no. 22, pp. 4380–4382, Nov. 2011.

[7] J. Villatoro, V. P. Minkovich, and D. Monzón-Hernández, "Temperature-independent strain sensor made from tapered holey optical fiber," *Opt. Lett.*, vol. 31, no. 3, pp. 305–307, Feb. 2006.

[8] Z. Tian and S. S. H. Yam, "In-line abrupt taper optical fiber Mach-Zehnder interferometric strain sensor," *IEEE Photon. Technol. Lett.*, vol. 21, no. 3, pp. 161–163, Feb. 2009.

[9] M. Hatta, Y. Semenova, Q. Wu, and G. Farrell, "Strain sensor based on a pair of single-mode-multimode-single-mode fiber structures in a ratiometric power measurement scheme," *Appl. Opt.*, vol. 49, no. 3, pp. 536–541, Jan. 2010.

[10] D. W. Duan, Y. J. Rao, Y. S. Hou, and T. Zhu, "Microbubble based fiber-optic fabry-perot interferometer formed by fusion splicing single-mode fibers for strain measurement," *Appl. Opt.*, vol. 51, no. 8, pp. 1033–1036, Mar. 2012.

[11] F. C. Favero, L. Araujo, G. Bouwmans, V. Finazzi, J. Villatoro, and V. Pruneri, "Spheroidal fabry-perot microcavities in optical fibers for high-sensitivity sensing," *Opt. Exp.*, vol. 20, no. 7, pp. 7112–7118, Mar. 2012.

[12] M. S. Yoon, S. Park, and Y. G. Han, "Simultaneous measurement of strain and temperature by using a micro-tapered fiber grating," *J. Lightw. Technol.*, vol. 30, no. 8, pp. 1156–1160, Apr. 2012.

[13] H. J. Patrick, A. D. Kersey, and F. Bucholtz, "Analysis of the response of long period fiber gratings to external index of refraction," *J. Lightw. Technol.*, vol. 16, no. 9, pp. 1606–1612, Sept. 1998.

[14] X. Shu, L. Zhang, and I. Bennion, "Sensitivity characteristics of long-period fiber gratings," *J. Lightw. Technol.*, vol. 20, no. 2, pp. 255–266, Feb. 2002.

[15] J. C. Guo, Y. S. Yu, X. L. Zhang, C. Chen, R. Yang, C. Wang, R. Z. Yang, Q. D. Chen, and H. B. Sun, "Compact long-period fiber gratings with resonance at second-order diffraction," *IEEE Photon. Technol. Lett.*, vol. 24, no. 16, pp. 1393–1395, Aug. 2012.
[16] Iadicicco, S. Campopiano, A. Cutolo, M. Giordano, and A. Cusano, "Refractive index sensor based on microstructured fiber bragg grating," *IEEE Photon. Technol. Lett.*, vol. 17, no. 6, pp. 1250–1252, June 2005.
[17] R. Yang, Y. S. Yu, C. Chen, Q. D. Chen, and H. B. Sun, "Rapid fabrication of microhole array structured optical fibers," *Opt. Lett.*, vol. 36, no. 19, pp. 3879–3881, Oct. 2011.
[18] S. M. Lee, M. Y. Jeong, and S. S. Saini, "Etched-core fiber bragg grating sensors integrated with microfluidic channels," *J. Lightw. Technol.*, vol. 30, no. 8, pp. 1025–1031, Apr. 2012.
[19] V. P. Minkovich, J. Villatoro, D. Monzón-Hernández, S. Calixto, A. B. Sotsky, and L. I. Sotskaya, "Holey fiber tapers with resonance transmission for high-resolution refractive index sensing," *Opt. Exp.*, vol. 13, no. 19, pp. 7609–7614, Sept. 2005.
[20] K. Q. Kieu and M. Mansuripur, "Biconical fiber taper sensors," *IEEE Photon. Technol. Lett.*, vol. 18, no. 21, pp. 2239–2241, Nov. 2006.
[21] Z. Tian and S. S. H. Yam, "In-line single-mode optical fiber interferometric refractive index sensors," *J. Lightw. Technol.*, vol. 27, no. 13, pp. 2296–2306, July 2009.
[22] P. Lu and Q. Chen, "Femtosecond laser microfabricated fiber Mach-Zehnder interferometer for sensing applications," *Opt. Lett.*, vol. 36, no. 2, pp. 268–270, Jan. 2011.
[23] D. Wu, T. Zhu, M. Deng, D. W. Duan, L. L. Shi, J. Yao, and Y. J. Rao, "Refractive index sensing based on Mach-Zehnder interferometer formed by three cascaded single-mode fiber tapers," *Appl. Opt.*, vol. 50, no. 11, pp. 1548–1553, Apr. 2011.
[24] J. Yang, L. Jiang, S. Wang, B. Li, M. Wang, H. Xiao, Y. Lu, and H. Tsai, "High sensitivity of taper-based Mach-Zehnder interferometer embedded in a thinned optical fiber for refractive index sensing," *Appl. Opt.*, vol. 50, no. 28, pp. 5503–5507, Oct. 2011.
[25] Z. Tian, S. S. H. Yam, and H. P. Loock, "Refractive index sensor based on an abrupt taper michelson interferometer in a single-mode fiber," *Opt. Lett.*, vol. 33, no. 10, pp. 1105–1107, May 2008.
[26] R. Yang, Y. S. Yu, Y. Xue, C. Chen, Q. D. Chen, and H. B. Sun, "Single S-tapered fiber Mach-Zehnder interferometers," *Opt. Lett.*, vol. 36, no. 23, pp. 4482–4484, Dec. 2011.
[27] L. C. Bobb, P. M. Shankar, and H. D. Krumboltz, "Bending effects in biconically tapered single-mode fibers," *J. Lightw. Technol.*, vol. 8, no. 7, pp. 1084–1090, July 1990.
[28] P. M. Shankar, L. C. Bobb, and H. D. Krumboltz, "Coupling of modes in bent biconically tapered single-mode fibers," *J. Lightw. Technol.*, vol. 9, no. 7, pp. 832–837, July 1991.
[29] J. D. Love, W. M. Henry, W. J. Stewart, R. J. Black, S. Lacroix, and F. Gonthier, "Tapered single-mode fibres and devices Part 1: Adiabaticity criteria," *Proc. Inst. Elect. Eng. J.*, vol. 138, no. 5, pp. 343–354, Oct. 1991.

Rui Yang received the B.S. degree in microelectronics from the College of Electronic Science and Engineering, Jilin University, Changchun, China, in 2009. He is currently pursuing the Ph.D. degree in the College of Electronic Science and Engineering, Jilin University.

His current research interests include femtosecond laser fabrication of fiber gratings and fiber optic sensors.

Yong-Sen Yu received the M.S. degree in electronics from Changchun University of Science and Technology, Changchun, China, in 2000, and the Ph.D. degree in the College of Electronic Science and Engineering from Jilin University, Changchun, China, in 2005.

In 2009, he worked as an Associate Professor in State Key Lab of Integrated Optoelectronics, Jilin University, Changchun, China. His current research interests include laser microfabrication, fiber gratings, and fiber optic sensors.

Chao Chen received the B.S. and the M.S. degrees in electronics science and technology from the College of Electronic Science and Engineering, Jilin University, Changchun, China, in 2005 and 2010, respectively. He is currently pursuing the Ph.D. degree in the College of Electronic Science and Engineering, Jilin University.

His current research interests include femtosecond laser fabrication of fiber gratings and fiber optic sensors. From July 2005 to August 2007, he worked as an engineer in Ibiden Electronics (Beijing) Co. Ltd.

Yang Xue received the B.S. degree in electronics science and technology from the College of Electronic Science and Engineering, Jilin University, Changchun, China, in 2011. He is currently pursuing the M.S. degree in the College of Electronic Science and Engineering, Jilin University.

His current research interests include femtosecond laser fabrication of fiber gratings and fiber optic sensors.

Xu-Lin Zhang received the B.S. degree in electronic information and science technology from the College of Electronic Science and Engineering, Jilin University, Changchun, China, in 2009, where he is currently working toward the Ph.D. degree.

His current research interests are in the area of transformation optics based optoelectronics devices.

Jing-Chun Guo received the B.S. degree in applied physics from the College of Physics, Jilin University, Changchun, China, in 2010. He is currently pursuing the M.S. degree in the College of Electronic Science and Engineering, Jilin University.

His current research interests include femtosecond laser fabrication of fiber gratings and fiber optic sensors.

Chuang Wang received the B.S. degree in electronics science and technology from the College of Electronic Science and Engineering, Jilin University, Changchun, China, in 2008. He is currently pursuing the M.S. degree in the College of Electronic Science and Engineering, Jilin University.

His current research interests include femtosecond laser fabrication of fiber gratings and fiber optic sensors.

Feng Zhu received the B.S. and the M.S. degrees in electronics science and technology from the College of Electronic Science and Engineering, Jilin University, Changchun, China, in 2003 and 2008, respectively. He is currently pursuing the Ph.D. degree in the College of Electronic Science and Engineering, Jilin University.

His current research interests include femtosecond laser fabrication of fiber gratings and fiber optic sensors.

Bao-Lin Zhang received the B.S. and the M.S. degrees in semiconductor physics and devices physics from the Department of Electronic Science, Jilin University, Changchun, China, in 1986 and 1989, respectively, and the Ph.D. degree in condensed matter physics from the Institute of Physics, Chinese Academy of Sciences, Changchun, China, in 1999.

He was doing post-doctorate research in the Department of Physics, University of Oxford, England, from 1999 to 2000, and then as a Researcher in Nanyang Technological University, Singapore, from 2001 to 2003. He is in charge of the MOCVD Laboratory, State Key Laboratory on Integrated Optoelectronics, Jilin University, China, from 2004 to the present and he is a Full Professor with Jilin University. His current research interests include wide band gap semiconductors (GaN, ZnO) and mid-infrared antimonide materials. So far, he has published over 70 scientific papers.

Qi-Dai Chen received the B.S. degree in physics from the University of Science and Technology of China, Hefei, China, in 1998, and the Ph.D. degree in the Institute of Physics, Chinese Academy of Sciences, Beijing, China, in 2004.

He was doing post-doctorate research at Osaka City University during 2005–2006. He is an Associate Professor with Jilin University. His current research interests include laser microfabrication, ultrafast laser spectroscopy, photochemistry, and photophysics.

Hong-Bo Sun received the B.S. and the Ph.D. degrees in electronics from Jilin University, Changchun, China, in 1992 and 1996, respectively.

He worked as a Postdoctoral Researcher in Satellite Venture Business Laboratory, University of Tokushima, Japan, from 1996 to 2000, and then as an Assistant Professor in the Department of Applied Physics, Osaka University, Osaka, Japan. In 2005, he was promoted as a Full Professor (Changjiang Scholar), Jilin University, China. His research has been focused on laser micro-nanofabrication in the past 10 years, particularly in exploring novel laser technologies including direct writing and holographic lithography, as well as their applications on microoptics, micromachines, microfluids, and microsensors. So far, he has published over 60 scientific papers in the above field, which have been cited for more than 3000 times according to ISI search report.

Prof. Sun became a project leader under PRESTO (Precursory Research for Embryonic Science and Technology, Japan) program in 2001, won National Natural Science Funds for Distinguished Young Scholar, China, in 2005, and his team was supported by PCSIRT (Program for Changjiang Scholars and Innovative Research Team at University, China) in 2007. He was awarded by Optical Science and Technology Society for his contribution to the technology of femtosecond laser initiated nanofabrication in 2002, and won Outstanding Young Scientist Award issued by the minister of MEXT (Ministry of Education, Culture, ports, Science & Technology, Japan) in 2006.